NATIONAL ADVISORY COMMITTEE FOR AERONAUTICS

TECHNICAL NOTE 1995

INFLUENCE OF WING FLEXIBILITY ON FORCE-TIME RELATION IN SHOCK STRUT FOLLOWING VERTICAL LANDING IMPACT

By Albert E. McPherson, J. Evans, Jr., and Samuel Levy

National Bureau of Standards

Washington
November 1949

NATIONAL ADVISORY COMMITTEE FOR AERONAUTICS

TECHNICAL NOTE 1995

INFLUENCE OF WING FLEXIBILITY ON FORCE-TIME RELATION IN SHOCK STRUT FOLLOWING VERTICAL LANDING IMPACT

By Albert E. McPherson, J. Evans, Jr., and Samuel Levy

SUMMARY

Tests were conducted to determine the force developed in a shock strut as a function of the flexibility of the attached wing structure. It was found that for a duration of impact T_I greater than 1.5 times the natural period T_N of the wing, the force-time relation in the shock strut was substantially the same as though the flexible structure had been replaced by a rigid body having the same net weight. The peak force for $1.5 < T_I/T_N < 2.5$ showed a reduction of up to 10 percent and the peak acceleration at the center, a reduction of up to 15 percent, due to flexibility. These reductions were somewhat greater than the probable experimental error of about 5 percent.

An analysis of the effect of wing flexibility on the impact force was also carried out. It was found that for $0.231 < T_I/T_N < 2.47$ and for $1 < M_1/M_0 < \infty$, where M_1 is the generalized mass of the wing in its fundamental mode and M_0 is its actual mass, the impact force for the flexible wing was 0.775 to 1.000 times that for the rigid wing. For current designs of large airplanes with $T_I/T_N \sim 1$ and $5 < M_1/M_0 < 15$, the impact force for the flexible wing would be about 0.95 times that for the rigid wing.

A formula, based on the analysis, is given for the ratio of impact force with a flexible wing to impact force with a rigid wing. This formula checks the experimental data within the experimental error.

INTRODUCTION

This report describes the second in a series of investigations at the National Bureau of Standards of impact force developed during landing of structural models. This research was initiated by the Bureau of Aeronautics, Department of the Navy, to provide an experimental check on analytical methods for determining the transient oscillations in the structure of an airplane during landing impact.

The first phase of this investigation (reference 1) describes tests in which measurements were made of the flexural transients in a model wing following vertical landing impact at a point below the center of gravity. It was found that the results were in good agreement with classical dynamics and in fair agreement with the statistical theory of Biot and Bisplinghoff (reference 2). Related work on the flexural-transients problem is being carried on in other laboratories and is partially described in the reports by Williams and Jones (reference 3), Zahorski (reference 4), Anderson (reference 5), Kramer (reference 6), Wasserman (reference 7), and Westfall (reference 8).

All the methods for predicting the flexural transients in an airplane structure presuppose a knowledge of the landing loads. These loads depend primarily on the inherent characteristics of the shock strut, the weight of the airplane, and the velocity of descent. An estimate of vertical loads based on these factors is given by Wasserman in reference 9.

Secondary influences on the vertical forces which develop during landing impact are the flexibility and mass distribution in the airplane. In large airplanes, where the period of the wing in its fundamental flexural mode is comparable with the duration of impact and where large masses may be supported by a relatively flexible structure, these effects may be significant. This paper presents the results of model tests and of a theoretical analysis to investigate these secondary effects.

An additional source of load discussed in detail by McBrearty (reference 10) is the drag force due to spin-up torque. McBrearty shows that this force may under adverse circumstances produce high dynamic response of the airplane. The coupling between these drag forces and the airplane flexibility will not be considered here, although it is likely that there is an interaction.

DESCRIPTION OF MODEL

The model (fig. 1) was designed to simulate an airplane consisting of fuselage, shock strut, and wing which is free to vibrate in its fundamental flexural mode. The combination of flexibly mounted wing masses ABA and rigidly mounted masses C of the model (fig. 1) can be replaced quickly by rigidly mounted masses A and B (fig. 2) having an equal total mass. In this way, tests with flexibly mounted and rigidly mounted masses could follow one another rapidly enough to eliminate errors caused by gradual changes in the electrical characteristics of the measuring system, in the damping constants of the shock strut, and in the resiliency of the "landing field."

The weight distribution in the model with flexible "wing" (fig. 1) was conveniently changed by removing the $\frac{1}{4}$-pound steel disks A from the end masses B and attaching them at studs D to the center of the model.

The shock strut used in the drop tests was the same as that used previously in connection with the tests of reference 1. It is shown in detail in figure 3. The shock strut is provided with eight valved ports in the damper to adjust the relation between damping force and displacement, and it is provided with springs of variable length to adjust the spring stiffness.

A vacuum-tube accelerometer E (figs. 1 and 2) is attached to the alighting gear to measure the acceleration of the center of the model. This accelerometer is described in reference 11. In addition, wire resistance strain gages were used together with a carrier-type bridge circuit and a six-channel oscillograph to measure the force transmitted by the springs, the damper, and the landing foot.

The mass distribution of the flexible wing and the stiffness of its cantilever springs F (fig. 1) were chosen to make the model dynamically equivalent to the simplified $\frac{1}{10}$-scale model of the B-24 airplane described in reference 1 in the sense that the relation between force and deflection at the center of the model was calculated to be nearly the same as that for the model of reference 1, assuming deflection of the wings in their fundamental flexural mode.

The stiffness and mass distribution of the models tested is shown in figure 4. The constant mass of the center section was in all cases equal to the mass of all of the solidly connected center section above the center line (G-G, fig. 1 and fig. 2) of the springs. Model B (fig. 4) corresponded most closely to the model of reference 1. Models A and C were tested to indicate the effect of small changes in the mass distribution. Model D, having the same total weight as the other models, but no flexibility, was tested to give an experimental solution for the extreme case of infinite rigidity.

DESCRIPTION OF TESTS

The model was dropped using the release gear shown in figure 7 of reference 1. The release gear supported the model only at two stations near the center since preliminary tests had shown that the initial strains due to the dead weight of the wing had a negligible effect on the impact force and acceleration at the alighting gear. The height of drop was about 0.7 inch.

Nine series of drop tests were made. The tests included all possible combinations of the three weight distributions (A, B, and C, fig. 4) with the following three landing conditions:

(a) A medium landing in which all eight ports controlling the flow of oil in the dashpot were opened one-fourth turn and the impact took place on a landing surface consisting of 3/4 inch of natural rubber covered by 1/4 inch of neoprene.

(b) A soft landing in which all eight ports were opened three-fourths turn and the impact surface was 1 inch of natural rubber.

(c) A hard landing in which ports 1 to 4 were opened one-half turn, ports 5 and 6 were opened one-fourth turn, and the surface was 1 inch of neoprene.

The test conditions for each one of the nine series of drops are summarized in table 1. In each series, the procedure was as follows. First, a drop was made in condition D (fig. 4); second, the mass distribution was changed as rapidly as possible to the desired condition (A, B, or C, fig. 4) and another drop was made; third, a repeat drop in condition D was made as a check on the test equipment; and last, the recording equipment was calibrated. The total time required for this sequence of drops was kept below 20 minutes to reduce possible errors arising from drift of the electrical equipment or changes in the characteristics of the damper or of the rubber and neoprene in the impact surface.

The drop records obtained are shown in figure 5. Curve I is a record of the acceleration at the center of the model, curve II is a record of the force transmitted through the fluid damper, curve III is a record of the force transmitted through the landing foot, and curve IV is a record of the force transmitted through the spring. Since it was not desired to include the decelerating forces for the foot fittings in the landing force, the force required to decelerate the model was taken as the sum of curves II and IV (fig. 5) rather than the somewhat larger force given by curve III.

The force acting on the landing foot was measured with wire strain gages attached to the 0.025-inch wall of an aluminum-alloy tube 3/4 inch in diameter supporting the landing foot (fig. 3). The spring force and the damper force were measured with wire-strain-gage pickups which are described in reference 1. These pickups were calibrated by recording the output corresponding to known static loads, as explained in reference 1. The scales derived from the calibrations are indicated on the records of figure 5. The records were measured in terms of these

scales with a traveling microscope. The results for the nine series of tests are shown in figures 6 to 14. The figures show that the wing flexibility used in the tests had only a minor effect on the shape of the force–time curve in most cases.

The peak impact forces developed are tabulated in columns (7), (8), and (9) of table 1. A comparison of the tests with and without wing is given in column (10), and a comparison for the two essentially identical tests without a wing is given in column (11). Except for series of drops 9, for which column (11) indicates excessive deviation from stable conditions of measurement, the wing flexibility caused a reduction in impact force of −2 to 10 percent. This reduction is of the same order of magnitude as the possible error of measurement, up to 6 percent, indicated by column (11) of table 1.

The impact acceleration at the center of the model was obtained from curves I in figure 5. The scale shown on the left end of these curves was obtained from the record itself by measuring the average deflection corresponding to the change in acceleration by 1g as the model is released. The accelerations were scaled from the record with a traveling microscope just as for the spring and damper forces. The results for the nine series of tests are shown in the right-hand portion of figures 6 to 14. Comparison of the dashed curves corresponding to no wing with the solid curve corresponding to a flexible wing shows that wing flexibility has a definite, though minor, effect on acceleration at the center. This effect is particularly noticeable for the drops having the shortest impact times (figs. 12 to 14).

The peak accelerations developed at the center are tabulated in columns (2), (3), and (4) of table 2. A comparison of the tests with and without wing is given in column (5) and a comparison of the two similar tests without wing is given in column (6). The effect of wing flexibility on center acceleration was to cause a reduction of 3 to 15 percent in the peak acceleration. This reduction is somewhat greater than the possible error of measurement of 5 percent indicated by column (6).

ANALYSIS

An analysis of the effect of wing flexibility on the forces developed in an idealized centrally located shock strut was made to obtain a more general solution than is possible with a limited number of tests, and to check the conclusions obtained from the tests that were made.

For the purpose of analysis, the airplane above the shock strut is also idealized as a body which has only two modes of motion, a rigid-body mode 0 and a fundamental mode of vibration 1, such as the fundamental free-free mode of the wing. The downward displacement y of the airplane at the point of impact corresponding to the point of attachment to the shock strut is then:

$$y_i = y_i^{(0)} + y_i^{(1)} \tag{1}$$

where

$y_i^{(0)}$ downward displacement of point of impact in rigid-body mode

$y_i^{(1)}$ downward displacement of point of impact in fundamental mode

The displacements $y_i^{(0)}$ and $y_i^{(1)}$ under the action of the upward impact force F are given by solving the equations developed on page 50 of reference 2:

$$\frac{d^2 y_i^{(0)}}{dt^2} = -\frac{F}{M_0} \tag{2}$$

$$\frac{d^2 y_i^{(1)}}{dt^2} + \omega^2 y_i^{(1)} = -\frac{F}{M_1} \tag{3}$$

where

M_0 mass of airplane

ω natural frequency in fundamental mode

t time

$$M_1 = \int \left(\frac{y^{(1)}}{y_i^{(1)}} \right)^2 dm \tag{3a}$$

where M_1 is the generalized mass of the airplane in the fundamental symmetrical mode, and $y^{(1)}$ is the deflection in this mode at the location of the element of mass dm.

The complicated action of the shock strut and tire of the alighting gear is approximated by that of the idealized system shown in figure 15. The constants k_2 and c, corresponding, respectively, to the springiness of the air chamber and damping action of the oil in the shock strut, are chosen by a cut-and-try procedure so that the peak force developed in one will be about equal to that developed in the other. This condition on the constants k_2 and c seemed reasonable since with a much larger value of c the impact would be too hard, while with a much smaller value no energy would be absorbed in the damper. In addition, this condition agrees approximately with the experimentally observed results for the model (see fig. 5). The constant k_1, corresponding to the springiness of the tire, is chosen by a cut-and-try procedure so that the maximum stroke developed in k_1 is about equal to that developed in k_2. The substitution of a linear spring for the tire was necessary to simplify the analysis. It was felt that such a substitution would be a fair approximation if the relative duration of impact and total travel for the tire and spring were about the same.

Applying the equations of equilibrium to the system shown in figure 15,

$$k_1 x = F \tag{4}$$

$$k_2(y_i - x) + c\left(\frac{dy_i}{dt} - \frac{dx}{dt}\right) = F \tag{5}$$

Substituting for F in equations (5), (2), and (3) the value in equation (4) and for y_i the value in equation (1), rearranging terms, and multiplying through by $(1/M_0\omega v)$, where v represents the downward velocity just prior to impact, give:

$$\left(\frac{k_1}{M_0\omega^2}\right)\left(\frac{x\omega}{v}\right) + \left(\frac{k_2}{M_0\omega^2}\right)\left(\frac{x\omega}{v} - \frac{y_i(0)\omega}{v} - \frac{y_i(1)\omega}{v}\right) +$$

$$\left(\frac{c}{M_0\omega}\right)\left(\frac{dx}{v\,dt} - \frac{dy_i(0)}{v\,dt} - \frac{dy_i(1)}{v\,dt}\right) = 0 \tag{6}$$

$$\left(\frac{k_1}{M_0\omega^2}\right)\left(\frac{x\omega}{v}\right) + \frac{d^2y_i(0)}{\omega v\,dt^2} = 0 \tag{7}$$

$$\left(\frac{k_1}{M_0\omega^2}\right)\left(\frac{x\omega}{v}\right) + \frac{M_1}{M_0}\left(\frac{\omega y_i^{(1)}}{v}\right) + \frac{M_1}{M_0}\left(\frac{d^2y_i^{(1)}}{\omega v\ dt^2}\right) = 0 \qquad (8)$$

Equations (6), (7), and (8) were solved both directly, using standard methods for solving simultaneous linear differential equations, and by numerical integration using Adam's method (pp. 363–367, reference 12). In both solutions, the initial conditions were taken as:

$$\left.\begin{aligned} x = 0, \quad & \frac{dx}{dt} = v \\ y_i^{(0)} = 0, \quad & \frac{dy_i^{(0)}}{dt} = v \\ y_i^{(1)} = 0, \quad & \frac{dy_i^{(1)}}{dt} = 0 \end{aligned}\right\} \quad (t = 0) \qquad (9)$$

Solutions were obtained for 16 cases covering a range of values of the dimensionless constants in equations (6), (7), and (8). The specific values are given in table 3 as follows: In column (2), the mass–distribution ratio M_1/M_0; in column (3), the ratio k_1/ω^2M_0; in column (4), the ratio k_2/ω^2M_0; and in column (5), the ratio $c/\omega M_0$.

Dimensionless displacement–time curves are presented in figures 16, 17, 18, and 19 for cases 2, 4, 6, and 14 of table 3, respectively. These cases all correspond to a mass–distribution ratio $M_1/M_0 = 5$ and a range of values of duration of impact to natural period T_I/T_N (column (6), table 3) from 2.47 to 0.30. The corresponding curves for other values of M_1/M_0 were similar to those shown for $M_1/M_0 = 5$. In cases 2, 4, 6, 7, 8, and 15, equations (6), (7), and (8) were solved both by the direct method for solving simultaneous linear differential equations and by numerical integration. The results agreed within 0.5 percent. Examination of the curves shows that the displacement $y_i^{(1)}$ in the fundamental mode is relatively small for long impacts (fig. 16), while for a sharp impact (fig. 19) it has a magnitude comparable with the total displacement.

Dimensionless impact force–time curves are presented in figures 20 and 21 for cases 4, 6, 8, and 9 of table 3. The dimensionless impact force was computed from the dimensionless displacement of the tire $x\omega/v$

and the ratios $k_1/\omega^2 M_0$ and $k_2/\omega^2 M_0$ given in table 3, by multiplying through equation (4) by the factor $\left(1/v\sqrt{k_2 M_0}\right)$, giving

$$\frac{F}{v\sqrt{k_2 M_0}} = \left(\frac{k_1}{\omega^2 M_0}\right)\left(\sqrt{\frac{\omega^2 M_0}{k_2}}\right)\left(\frac{x\omega}{v}\right)$$

It is seen that the rising portion of the curves is similar in shape in the four cases. Case 9 shows a marked difference near the end in maintaining a small force for a somewhat longer time. The effect on the force–time curve of changing only the mass-distribution ratio M_1/M_0 from 3 to 5 is seen by comparing the pairs of curves in figures 20 and 21. The effect is small over a major portion of the impact.

Dimensionless curves of impact force against time are presented in figure 22 for all the cases in table 3. The dimensionless ratios $F/v\sqrt{k_2 M_0}$ and $t\sqrt{k_2 M_0}$ used in figure 22 were selected since they are unaffected by either ω or M_1 and thus make it possible to plot all the cases on a single figure, bringing out the effects on the force–time curve of both natural frequency and mass distribution. The natural frequency for the different cases is given in column (7) of table 3 as the dimensionless ratio $\omega\sqrt{M_0/k_2}$. The spring ratio k_1/k_2 of the alighting gear (column (8), table 3) was 2 for all the cases investigated; while the damping ratio $c/\sqrt{k_2 M_0}$ of the oil chamber (column (9), table 3) was 1 for the first 11 cases and 1.414 for the remaining 5 cases. Comparison of the curves for the two sets of cases shows that changes in flexibility and in mass distribution had a marked effect on the force–time curve. The effect was most pronounced when the mass-distribution ratio M_1/M_0 had a relatively low value, cases 11 and 16. The effect of increasing $c/\sqrt{k_2 M_0}$ from 1 to 1.414 was to increase the peak impact force about 10 percent and cause a corresponding reduction in the duration of impact.

The peak values of the force ratio $\left(F/v\sqrt{k_2 M_0}\right)_{max}$ are tabulated in column (10) of table 3. The ratio of the peak value $\left(F/v\sqrt{k_2 M_0}\right)_{max}$ for a particular case to the value when $M_1/M_0 = \infty$ (everything else being kept constant) was taken as the ratio F_F/F_R of impact force for a flexible wing to impact force for a rigid wing. Values of F_F/F_R are tabulated in column (11). The ratio T_I/T_N of duration of impact to the natural period of the wing in its fundamental flexural mode is given in column (6).

The effect of wing flexibility alone is seen by comparing with each other the results for cases 2, 4, and 6, for which $M_1/M_0 = 5$ or those for cases 7, 8, and 9, for which $M_1/M_0 = 3$. For cases 2, 4, and 6 with $M_1/M_0 = 5$, the duration of impact ratio varies from 2.468 to 0.535 while the impact-force ratio F_F/F_R drops from 0.998 to 0.938. For cases 7, 8, and 9 with $M_1/M_0 = 3$, the duration of impact ratio drops from 2.468 to 0.788 while the impact-force ratio drops from 0.997 to 0.900. For case 14 with $M_1/M_0 = 5$ and with k_1/k_2 the same as for cases 1, 3, and 5 but with $c/\sqrt{k_2 M_0}$ larger by 0.414, the duration of impact-force ratio is 0.937. For case 15 with $M_1/M_0 = 3$ and with k_1/k_2 and $c/\sqrt{k_2 M_0}$ the same as for case 14, the duration of impact ratio is 0.290 when the impact-force ratio is 0.902. Wing flexibility in all cases results in a reduction of impact force. The magnitude of the reduction depends also on the ratio M_1/M_0.

The effect of mass-distribution ratio M_1/M_0 is also seen in table 3. Comparing with each other the results for cases 1, 2, and 7 corresponding to a duration of impact ratio of about 2.47 shows that, for a range of values of M_1/M_0 from ∞ to 3, the impact-force ratio drops from 1.000 to 0.997. Similarly, for cases 3, 4, and 8 corresponding to a duration of impact ratio of about 1.26, a variation of values of M_1/M_0 from ∞ to 3 gives a variation of impact-force ratios from 1.000 to 0.931. For cases 5, 6, and 9 corresponding to a duration of impact ratio of 0.5 to 0.8, a variation of values of M_1/M_0 from ∞ to 3 gives a variation of impact-force ratios from 1.000 to 0.900. For cases 12 to 16 corresponding to a duration of impact ratio of 0.2 to 0.3, a variation of M_1/M_0 from ∞ to 1 gives a variation of impact-force ratios from 1.000 to 0.780. Reduction of the mass-distribution ratio M_1/M_0 results in a reduction of the impact-force ratio. The magnitude of the reduction depends on the value of the duration of impact ratio.

The results for the impact-force ratio F_F/F_R given in column (11) of table 3 can be described, within 2 percent over the range indicated, by the following approximate relations:

$$\left.\begin{aligned} F_F/F_R &= 1 - 0.16\left(1 - \frac{M_1}{12M_0}\right)\left(1 - \frac{T_I}{2.5T_N}\right) \\ &\text{for } 2.5 < M_1/M_0 < 12 \text{ and } 0.4 < T_I/T_N < 2.5 \\ F_F/F_R &= 1 \\ &\text{for } M_1/M_0 > 12 \text{ or } T_I/T_N > 2.5 \end{aligned}\right\} \quad (10)$$

where

F_F impact force on flexible wing

F_R impact force on rigid wing of same total mass

M_1 generalized mass in fundamental mode (see equation (3a))

M_0 total mass

T_I duration of impact

T_N natural period of fundamental flexural mode of wing

COMPARISON OF EXPERIMENT AND ANALYSIS

The experimental results in table 1 have been retabulated in table 4 for comparison with values computed from equation (10). Such an over-all check of equation (10) seemed essential because of the many simplifying assumptions made in deriving it. In computing from equation (10), T_I was taken as the value in column (5) of table 1, T_N as the value in column (2). The values of M_1/M_0 for the different mass distributions in figure 4 were computed from equation (3a) and found to be 5.06 for case A, 3.72 for case B, and 2.87 for case C. Series of drops 9 (table 1) was omitted from the comparison because column (11) in that table indicates a much larger error in the recorded values than for the previous drops. The experimental and calculated results in table 4 agree within 5 percent except for series of drops 3, which differed by 7 percent. These differences are of the same order of magnitude as those indicated for the experimental error (column (11), table 1).

CONCLUSIONS

Both experiment and analysis indicate that wing flexibility has some effect on the shape and peak value of the force–time curve in a shock strut. However, the effect was significant (greater than 6 percent on peak value) only for values of duration of impact ratio $T_I/T_N < 1$ and mass–distribution ratio $M_1/M_0 < 5$.

The flexibility caused a reduction of the peak value of force in all cases studied analytically and, within the margin of experimental error, in all cases studied experimentally. This indicates that the effect of wing flexibility on shock–strut force may be neglected in the design of conventional airplanes without reducing the margin of safety.

National Bureau of Standards
Washington, D. C., August 23, 1948

REFERENCES

1. Ramberg, Walter, and McPherson, Albert E.: Experimental Verification of Theory of Landing Impact. Res. Paper RP1936, Jour. Res. Nat. Bur. Standards, vol. 41, no. 5, Nov. 1948, pp. 509–520.

2. Biot, M. A., and Bisplinghoff, R. L.: Dynamic Loads on Airplane Structures during Landing. NACA ARR 4H10, 1944.

3. Williams, D., and Jones, R. T. N.: Dynamic Loads in Airplanes under Given Impulse Loads with Particular Reference to Landing and Gust Loads on a Large Flying Boat. R. & M. No. 2221, British A.R.C., 1948.

4. Zahorski, Adam T.: Free Vibrations of Sweptback Wing. Jour. Aero. Sci., vol. 14, no. 12, Dec. 1947, pp. 683–692.

5. Anderson, Roger A.: Determination of Coupled Modes and Frequencies of Swept Wings by Use of Power Series. NACA RM L7H28, 1947.

6. Kramer, E. H.: Dynamic Loads on Wings with Tip Weights during Landing, Taxiing and Take-Off. USAF Air Materiel Command, Eng. Div. Memo. Rep. TSEAC5-45128-2-15, Aug. 1, 1947.

7. Wasserman, Lee S.: A Simplified Procedure for Computing Transient Responses of Linear Systems to Landing Gear Impulses. USAF Air Materiel Command, Eng. Div. Memo. Rep. TSEAC5-4595-5-4, Aug. 8, 1947.

8. Westfall, John R.: Measurements of Landing-Gear Forces and Horizontal-Tail Loads in Landing Tests of a Large Bomber-Type Airplane. NACA TN 1140, 1946.

9. Wasserman, Lee S.: Estimation of Vertical Loads in Landing Gears. USAF Air Materiel Command, Eng. Div. Memo. Rep. TSEAC5-4595-5-5, Aug. 8, 1947.

10. McBrearty, J. F.: A Critical Study of Aircraft Landing Gears. Jour. Aero. Sci., vol. 15, no. 5, May 1948, pp. 263–280.

11. Ramberg, Walter: Vacuum-Tube Acceleration Pickup. Res. Paper RP 1754, Jour. Res. Nat. Bur. Standards, vol. 37, no. 6, Dec. 1946, pp. 391–398.

12. Whittaker, E. T., and Robinson, G.: The Calculus of Observations. Fourth ed., Blackie and Son, Ltd. (London), 1944.

TABLE 1.- PEAK IMPACT FORCE DEVELOPED IN DROP TESTS AND COMPARISON BETWEEN DROPS WITH AND WITHOUT WING

(1)	(2)	(3)	(4)	(5)	(6)	(7)	(8)	(9)	(10)	(11)
Series of drops	Model		Total weight (lb)	Landing condition		Peak impact force developed (lb)			Run 2 / Av. of runs 1 and 3 (percent)	Experimental error for runs 1 and 3 (percent)
	Natural period (sec)	Type (fig. 4)		Approx. duration (sec)	Type (1)	Run 1 (without wing) (lb)	Run 2 (with wing) (lb)	Run 3 (without wing) (lb)		
1	0.028	A	42.70	0.064	a	207	206	207	100	0
2	.031	B	42.70	.063	a	225	205	216	93	4
3	.034	C	42.70	.064	a	216	194	216	90	0
4	.028	A	42.70	.069	b	192	191	203	97	6
5	.031	B	42.70	.071	b	178	180	184	99	3
6	.034	C	42.70	.075	b	188	183	191	96	2
7	.028	A	42.70	.050	c	251	260	260	102	4
8	.031	B	42.70	.051	c	285	268	270	96	5
9	.034	C	42.70	.051	c	276	200	244	77	12

[1]The landing conditions were as follows:

a, medium landing: all eight ports in damper open one-fourth turn, landing surface consisted of 3/4 inch of natural rubber topped by 1/4 inch of neoprene.

b, soft landing: all ports open three-fourths turn; landing surface, 1 inch of natural rubber.

c, hard landing: ports 1 to 4 at one-half turn; ports 5 and 6 at one-fourth turn; ports 7 and 8 closed; landing surface, 1 inch of neoprene.

TABLE 2.- PEAK ACCELERATION DEVELOPED AT CENTER IN DROP TESTS AND COMPARISON BETWEEN DROPS WITH AND WITHOUT FLEXIBLE WING

(1)	(2)	(3)	(4)	(5)	(6)
Series of drops	Peak acceleration (g)			Run 2 / Av. of runs 1 and 3 (percent)	Experimental error for runs 1 and 3 (percent)
	Run 1 (without wing)	Run 2 (with wing)	Run 3 (without wing)		
1	5.37	5.09	5.32	95	1
2	5.49	5.01	5.51	91	0
3	5.58	5.16	5.62	92	1
4	4.80	4.65	5.04	94	5
5	4.66	4.39	4.85	92	4
6	4.88	4.17	4.92	85	1
7	6.27	6.05	6.26	97	0
8	6.59	6.12	6.37	94	3
9	6.42	6.15	6.28	97	2

TABLE 3.- COMPUTED EFFECT OF WING FLEXIBILITY AND MASS DISTRIBUTION ON IMPACT FORCE

(1)	(2)	(3)	(4)	(5)	(6)	(7)	(8)	(9)	(10)	(11)
Case	Mass-distribution ratio, M_1/M_0	$\frac{k_1}{\omega^2 M_0}$	$\frac{k_2}{\omega^2 M_0}$	$\frac{c}{\omega M_0}$	Duration of impact ratio, T_I/T_N	Natural-frequency ratio, $\omega\sqrt{M_0/k_2}$	Spring ratio, k_1/k_2	Damping ratio, $c/\sqrt{k_2 M_0}$	Max. force ratio, $\left(\frac{F}{v\sqrt{k_2 M_0}}\right)_{max}$	Impact force ratio, F_F/F_R (a)
[b]1	∞	0.08	0.04	0.2	2.468	5	2	1	0.802	1.000
2	5	.08	.04	.2	2.468	5	2	1	.800	.998
[c]2	5	.08	.04	.2	2.463	5	2	1	.798	.995
[b]3	∞	.32	.16	.4	1.234	2.5	2	1	.802	1.000
4	5	.32	.16	.4	1.257	2.5	2	1	.768	.958
[c]4	5	.32	.16	.4	1.261	2.5	2	1	.769	.959
[b]5	∞	2.00	1.00	1.00	.494	1	2	1	.802	1.000
6	5	2.00	1.00	1.00	.535	1	2	1	.752	.938
[c]6	5	2.00	1.00	1.00	.535	1	2	1	.751	.937
7	3	.08	.04	.2	2.468	5	2	1	.799	.997
[c]7	3	.08	.04	.2	2.474	5	2	1	.795	.992
8	3	.32	.16	.4	1.274	2.5	2	1	.747	.931
[c]8	3	.32	.16	.4	1.271	2.5	2	1	.747	.931
9	3	2.00	1.00	1.00	.788	1	2	1	.722	.900
10	10	2.00	1.00	1.00	.505	1	2	1	.775	.967
11	1	2.00	1.00	1.00	.844	1	2	1	.622	.775
12	∞	4.00	2.00	2.00	.315	.707	2	1.414	.876	1.000
13	10	4.00	2.00	2.00	.307	.707	2	1.414	.846	.966
14	5	4.00	2.00	2.00	.299	.707	2	1.414	.820	.937
15	3	4.00	2.00	2.00	.290	.707	2	1.414	.789	.902
[c]15	3	4.00	2.00	2.00	.288	.707	2	1.414	.794	.907
16	1	4.00	2.00	2.00	.231	.707	2	1.414	.683	.780

[a]In calculating this ratio, use was made of the fact that the performance of a wing with finite ω and $M_1/M_0 = \infty$ is the same as that of a wing with finite M_1/M_0 and $\omega = \infty$ for the same value of M_0 and the landing-gear constants k_1, k_2, and c.

[b]Cases 1 and 3 were obtained from case 5 by changing ω.

[c]Cases solved by methods of differential equations, other cases by numerical integration.

TABLE 4.- COMPARISON OF EXPERIMENTAL VALUES OF IMPACT FORCE WITH AND WITHOUT FLEXIBLE WING WITH COMPUTED VALUES

(1)	(2)	(3)	(4)	(5)	(6)
Series of drops	Duration of impact ratio, T_1/T_N	Mass-distribution ratio, M_1/M_0	Impact-force ratio		Difference (percent)
			Measured (table 1, column (10)), F_F/F_R (percent)	Computed (equation (10)), F_F/F_R (percent)	
1	2.29	5.06	100	99	1
2	2.03	3.72	93	98	-5
3	1.88	2.87	90	97	-7
4	2.46	5.06	97	100	-3
5	2.29	3.72	99	99	0
6	2.20	2.87	96	99	-3
7	1.79	5.06	102	97	5
8	1.64	3.72	96	96	0

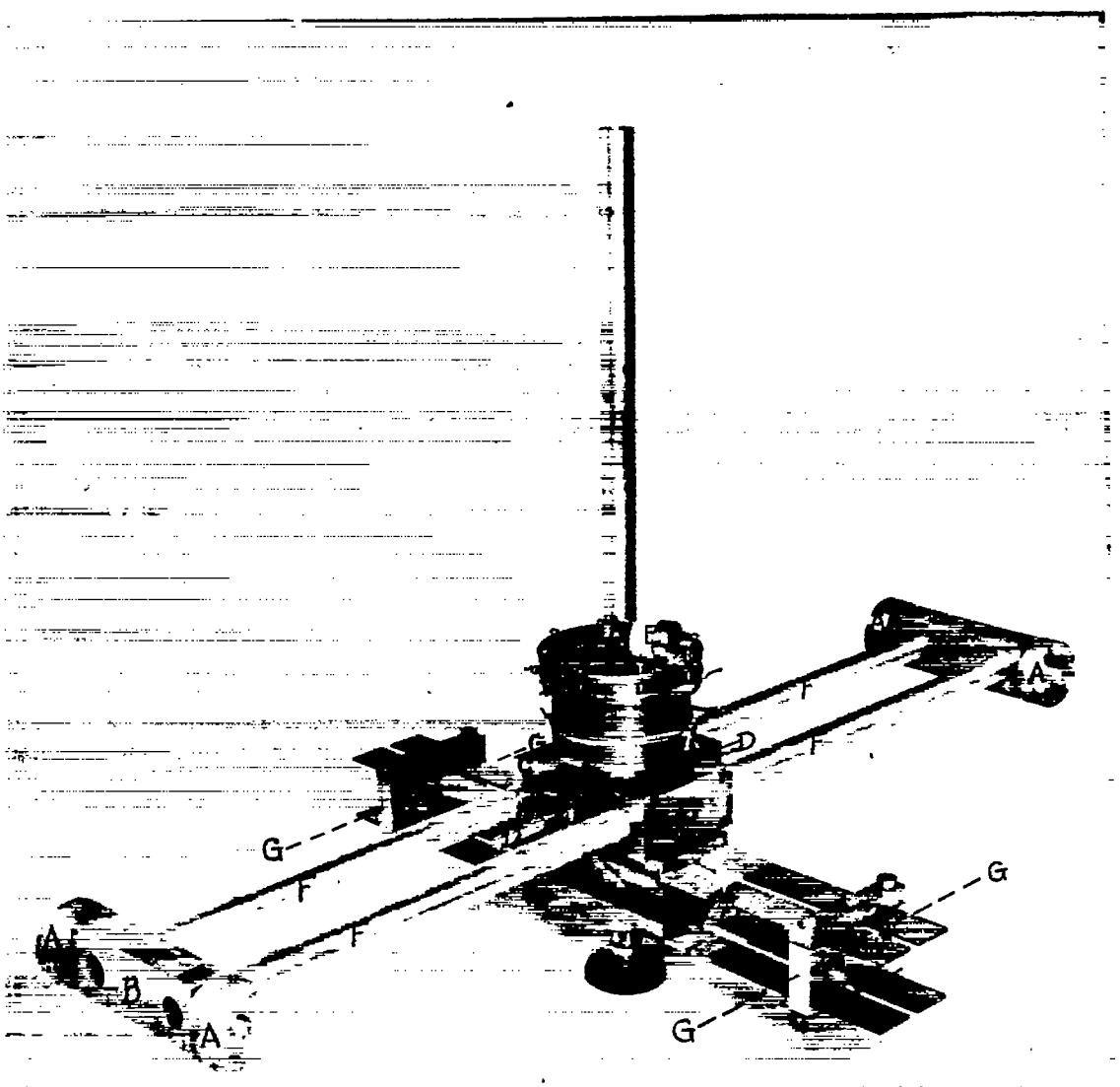

Figure 1.- Model with flexible wing.

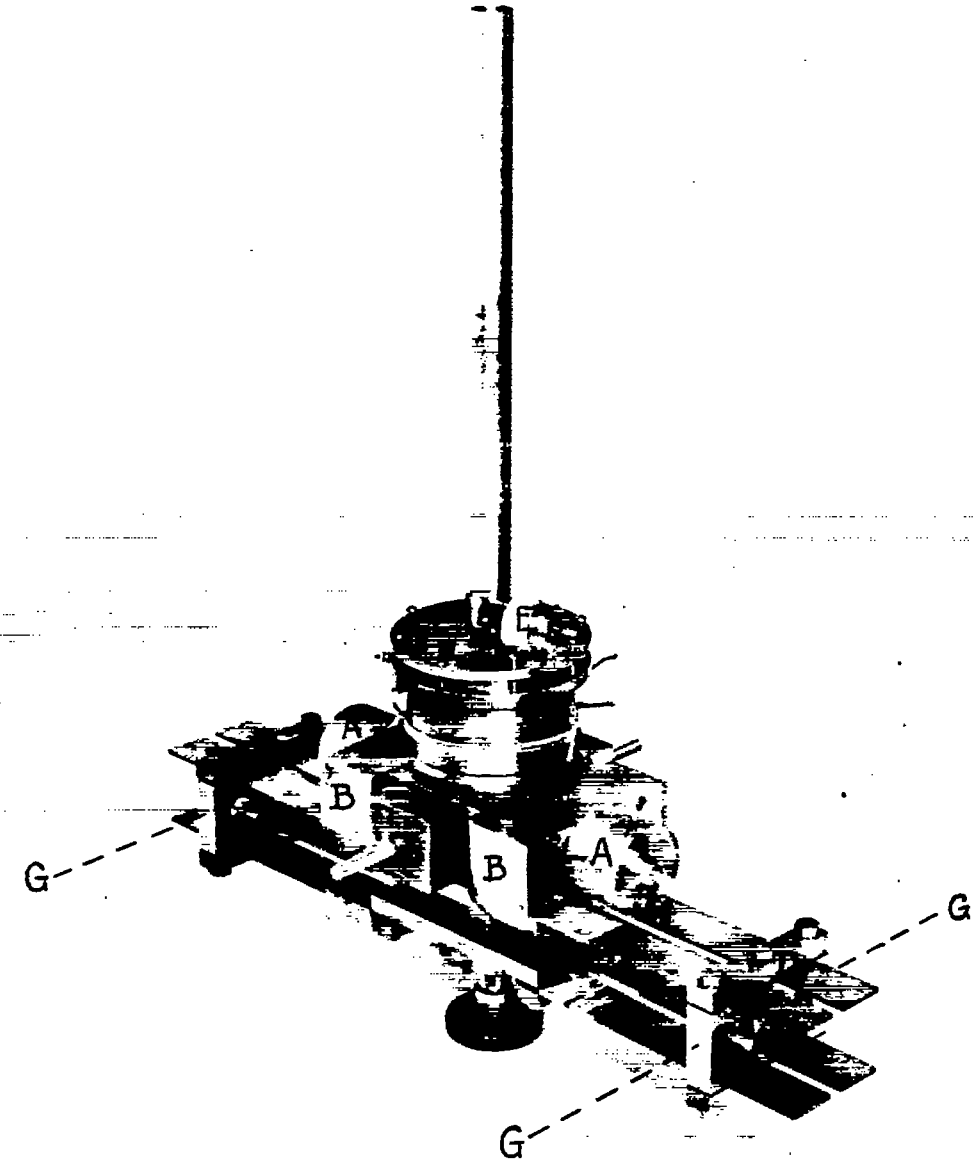

Figure 2.- Model with rigid wing.

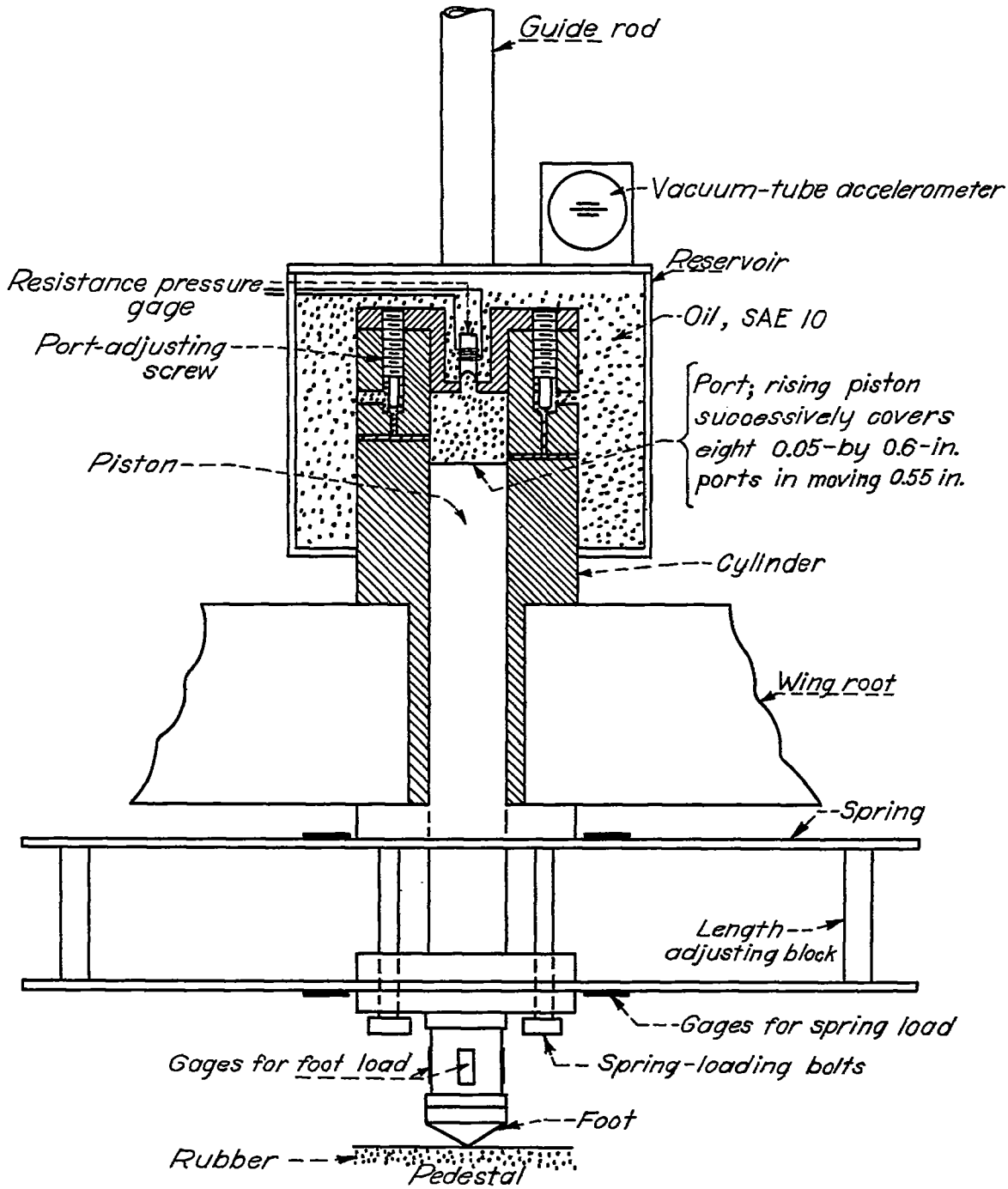

Figure 3.- Schematic diagram of alighting gear.

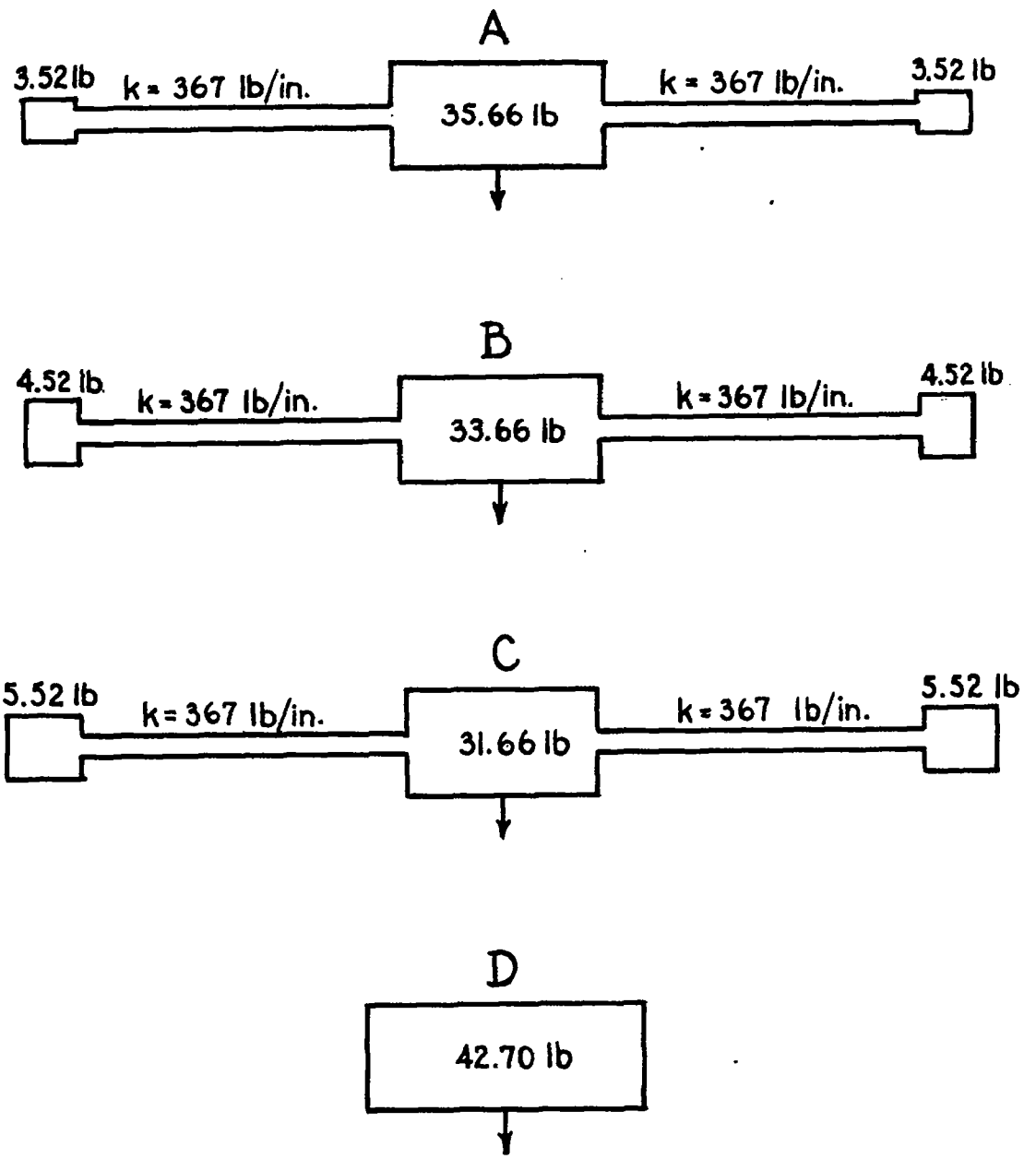

Figure 4.- Schematic view showing stiffness k and mass distribution of models tested.

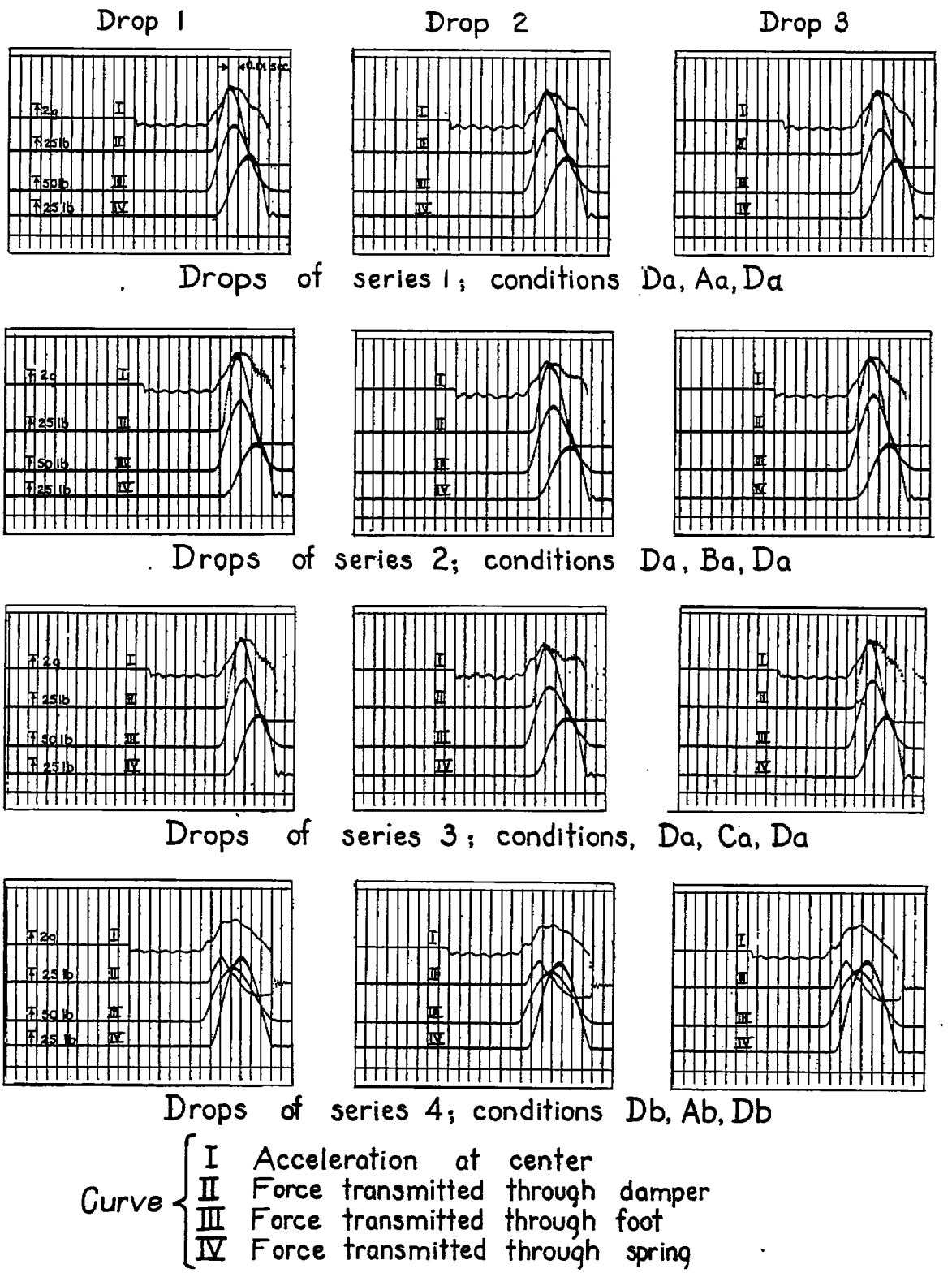

Figure 5.- Records obtained in drop tests. (See table 1.)

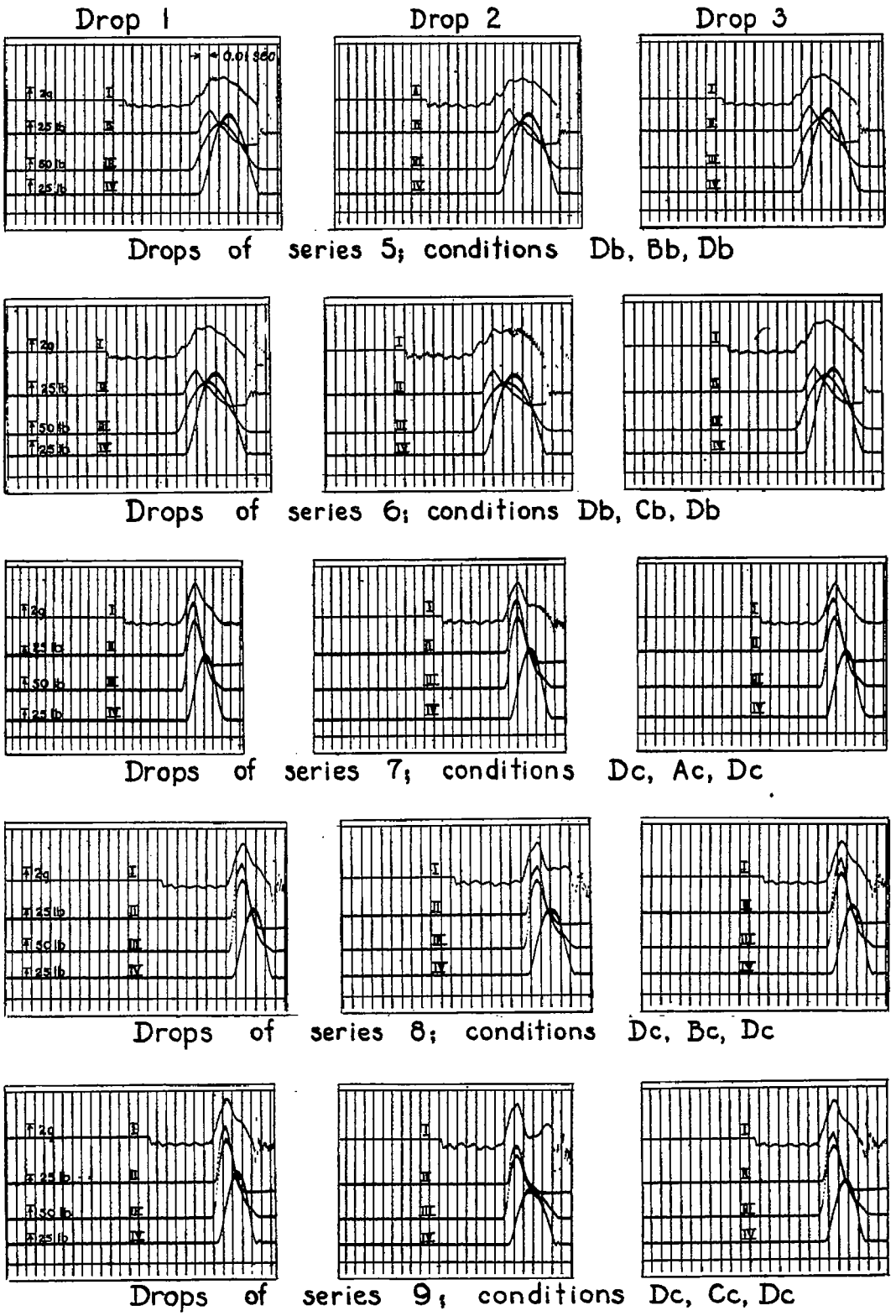

Figure 5.- Concluded.

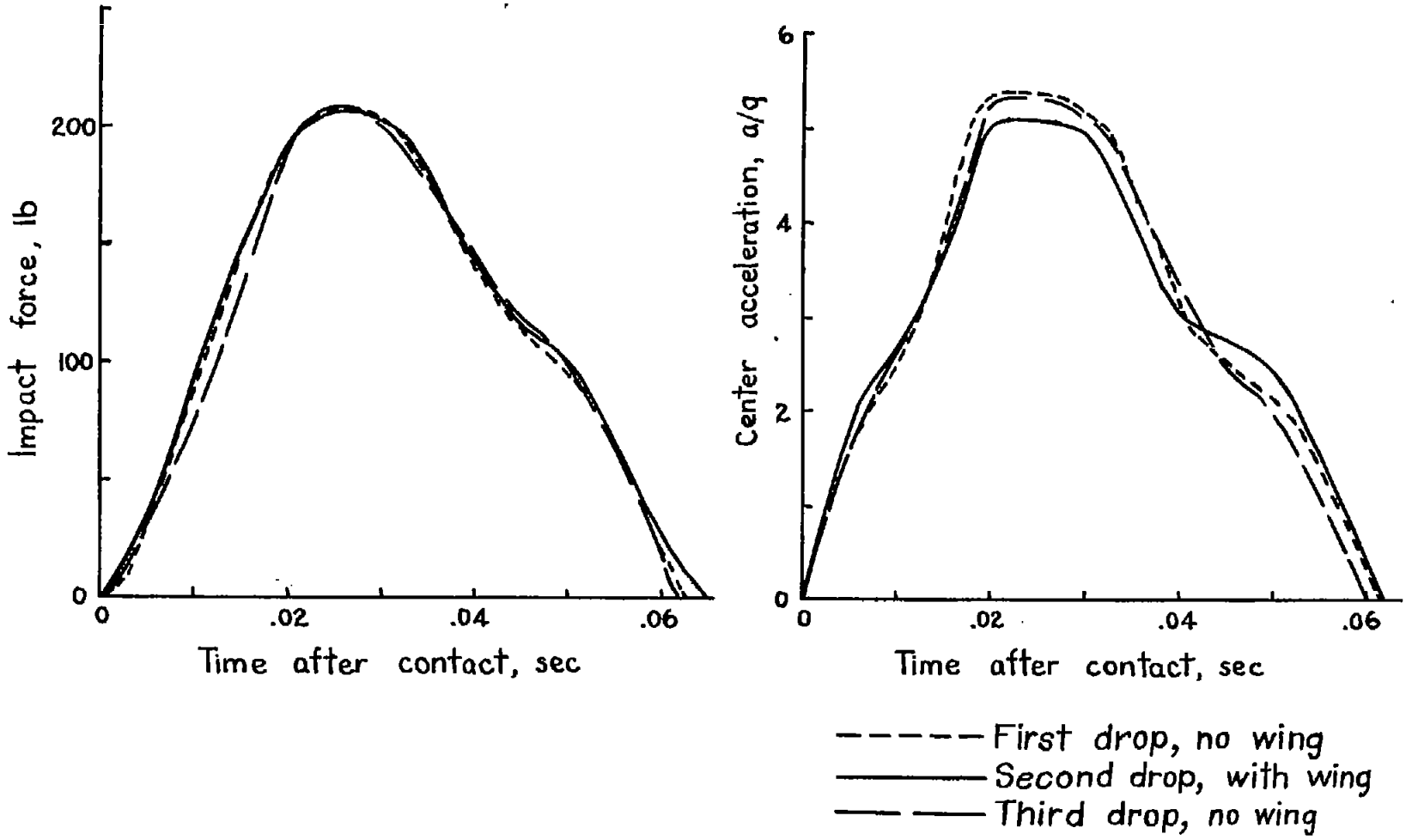

Figure 6.- Impact force and center acceleration in drops of series 1. Condition Aa, 3.52 pounds at wing tip, medium landing.

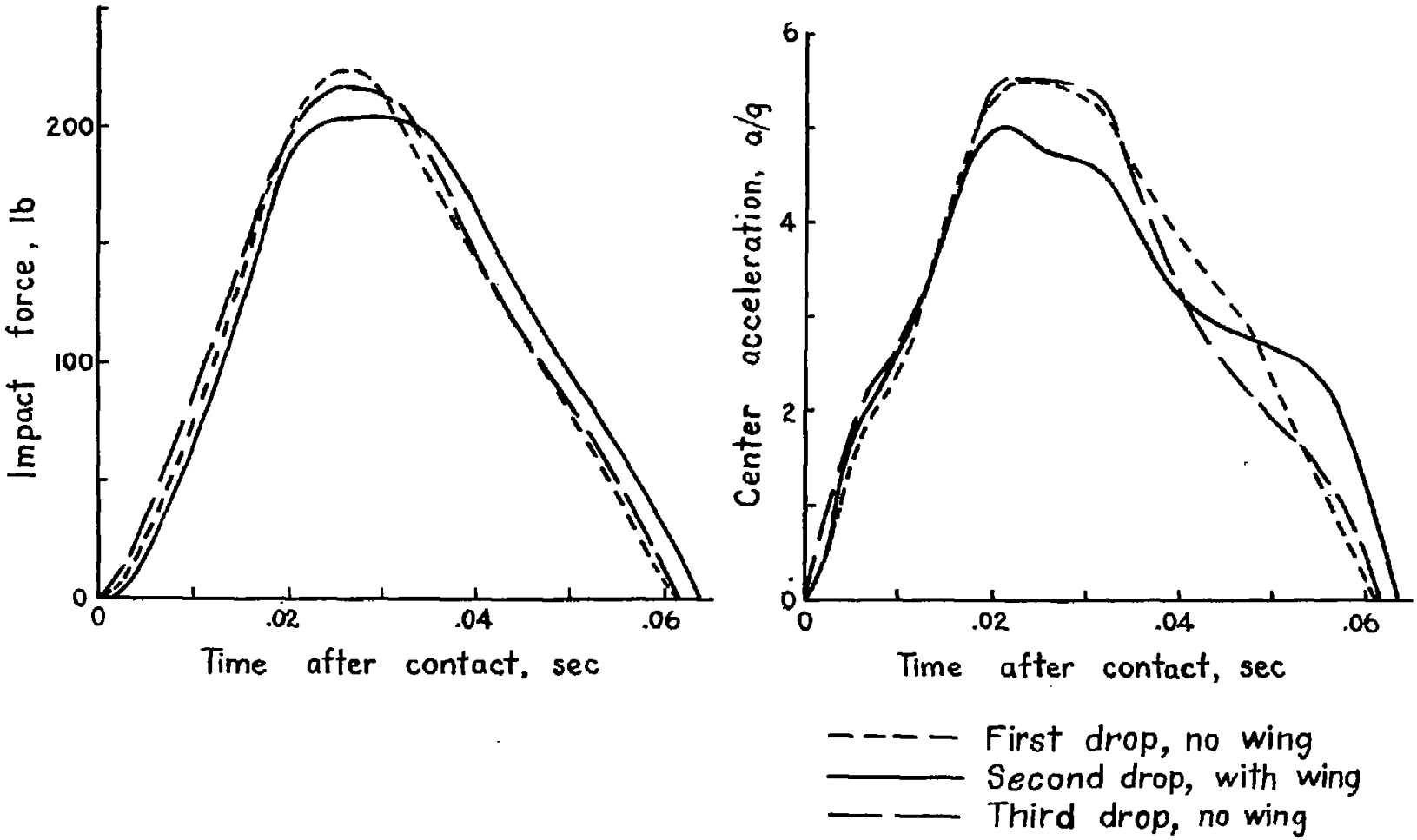

Figure 7.- Impact force and center acceleration in drops of series 2. Condition Ba, 4.52 pounds at wing tip, medium landing.

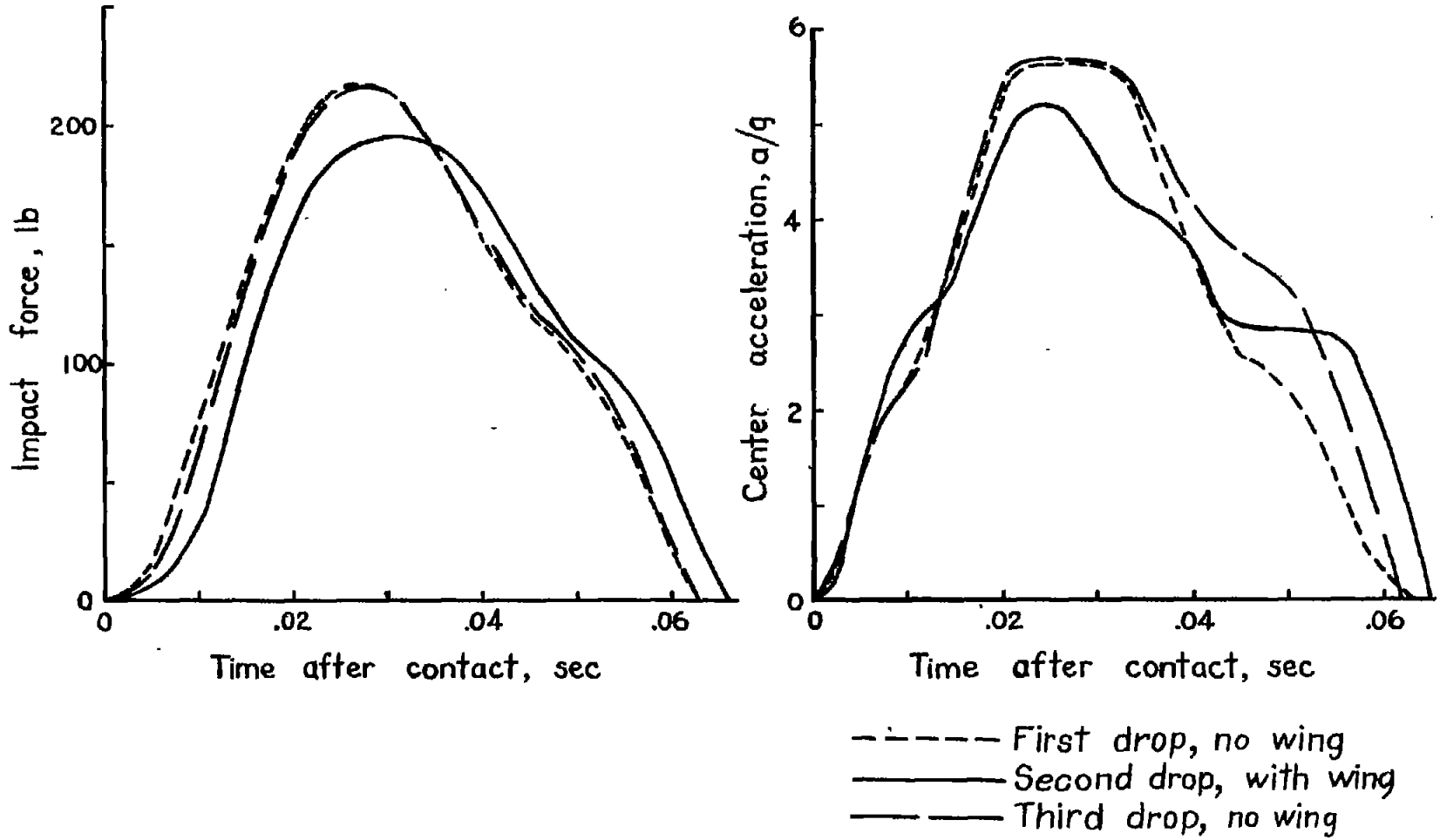

Figure 8.- Impact force and center acceleration in drops of series 3. Condition Ca, 5.52 pounds at wing tip, medium landing.

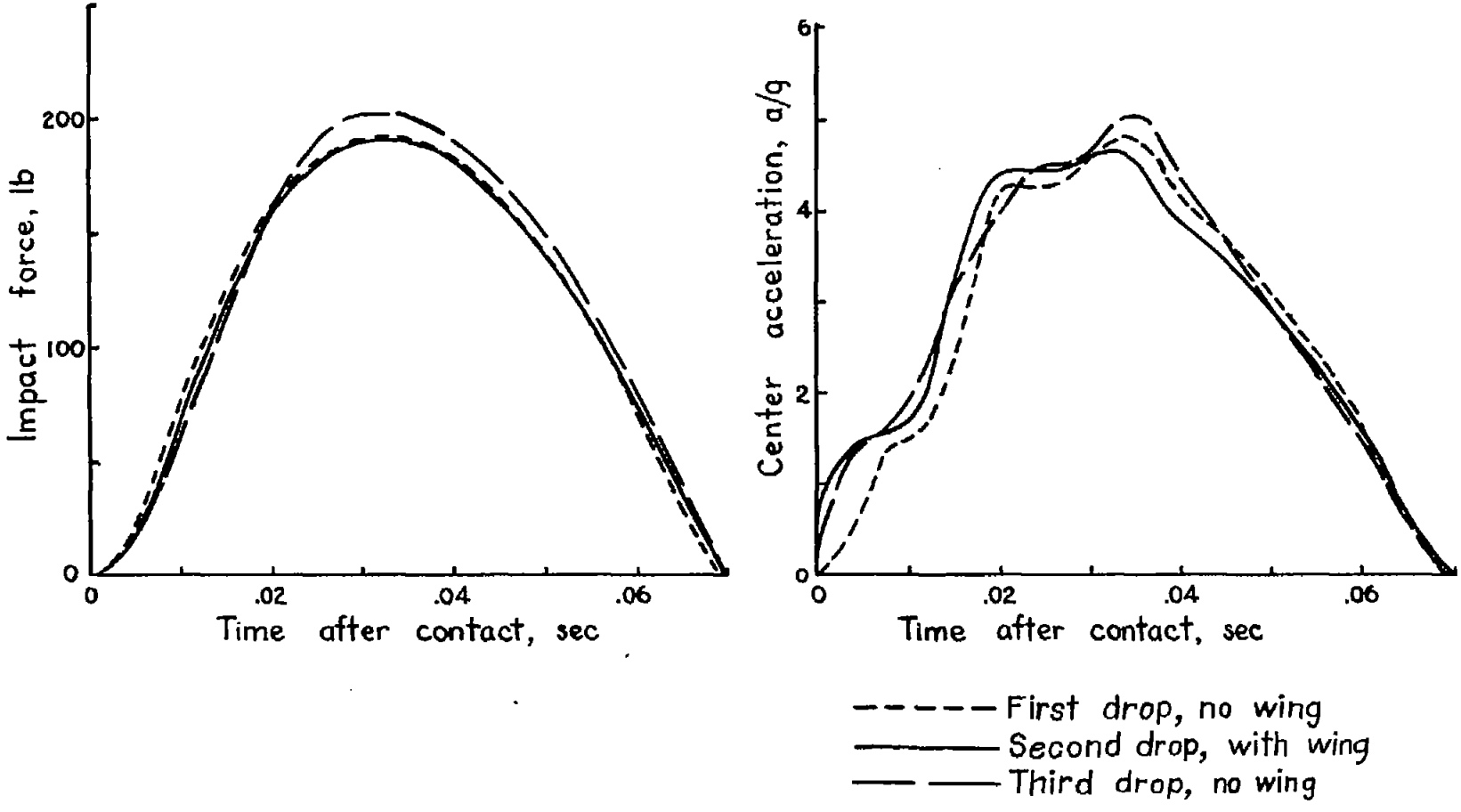

Figure 9.- Impact force and center acceleration in drops of series 4. Condition Ab, 3.52 pounds at wing tip, soft landing.

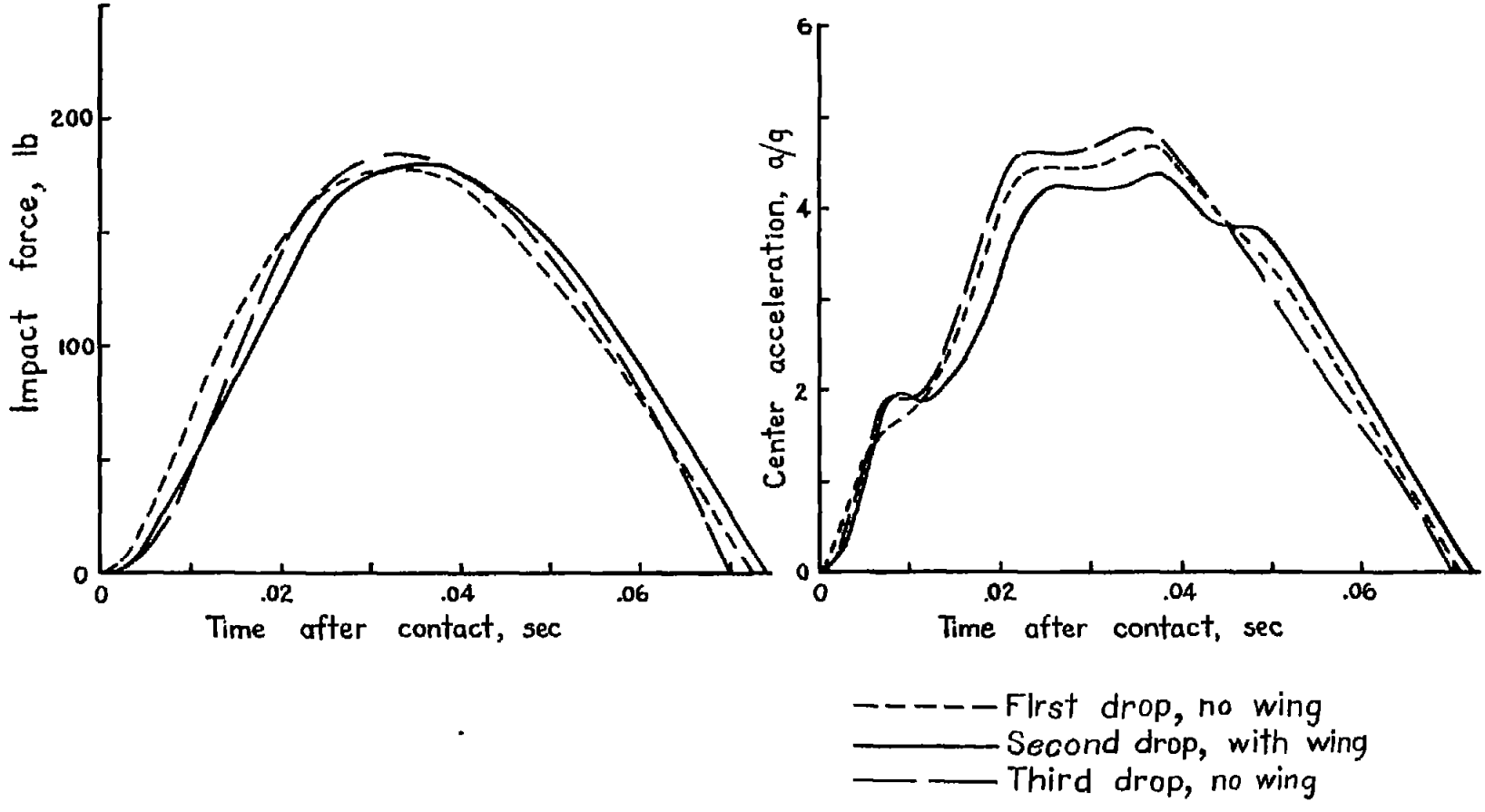

Figure 10.- Impact force and center acceleration in drops of series 5. Condition Bb, 4.52 pounds at wing tip, soft landing.

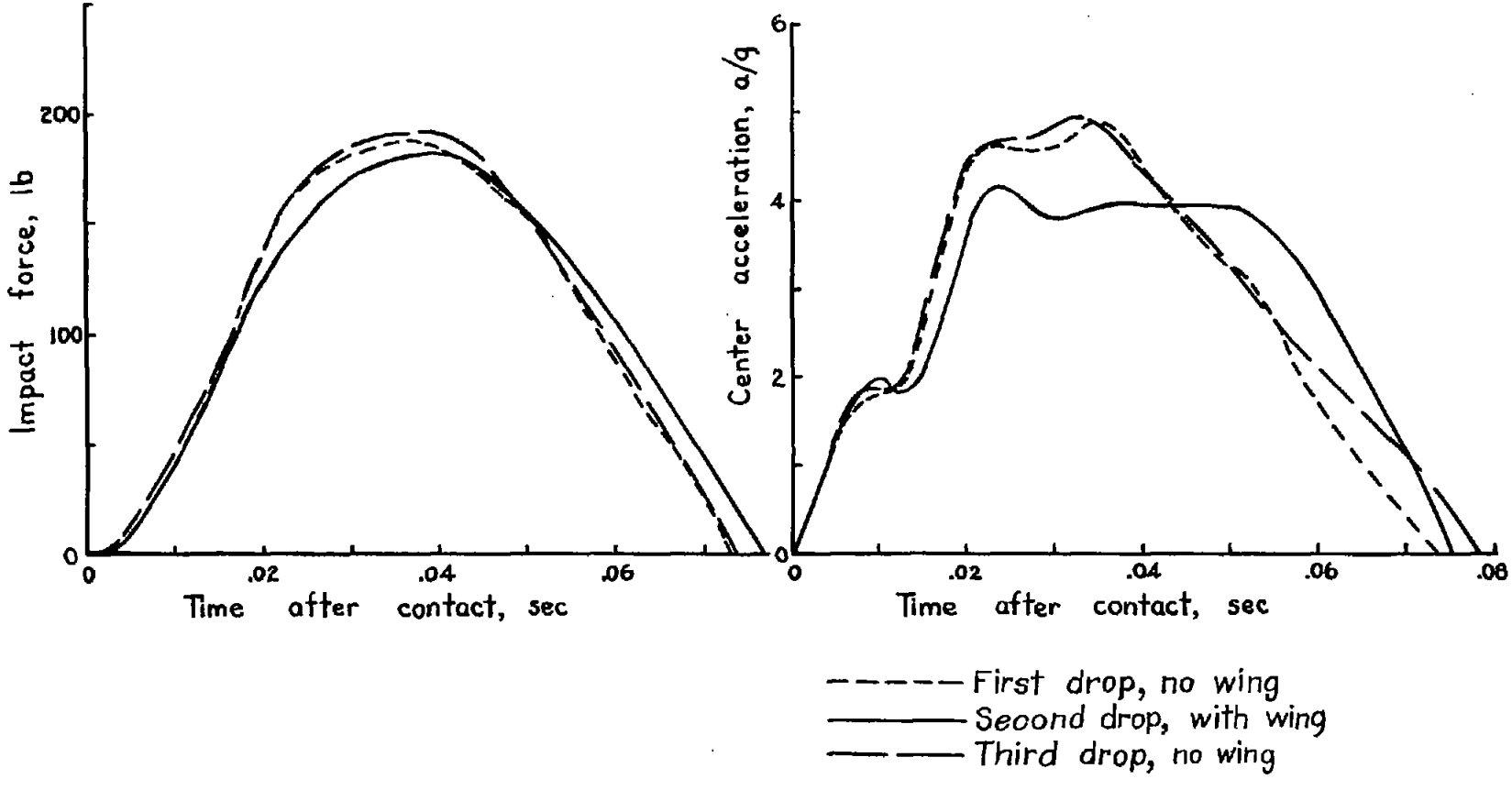

Figure 11.- Impact force and center acceleration in drops of series 6. Condition Cb, 5.52 pounds at wing tip, soft landing.

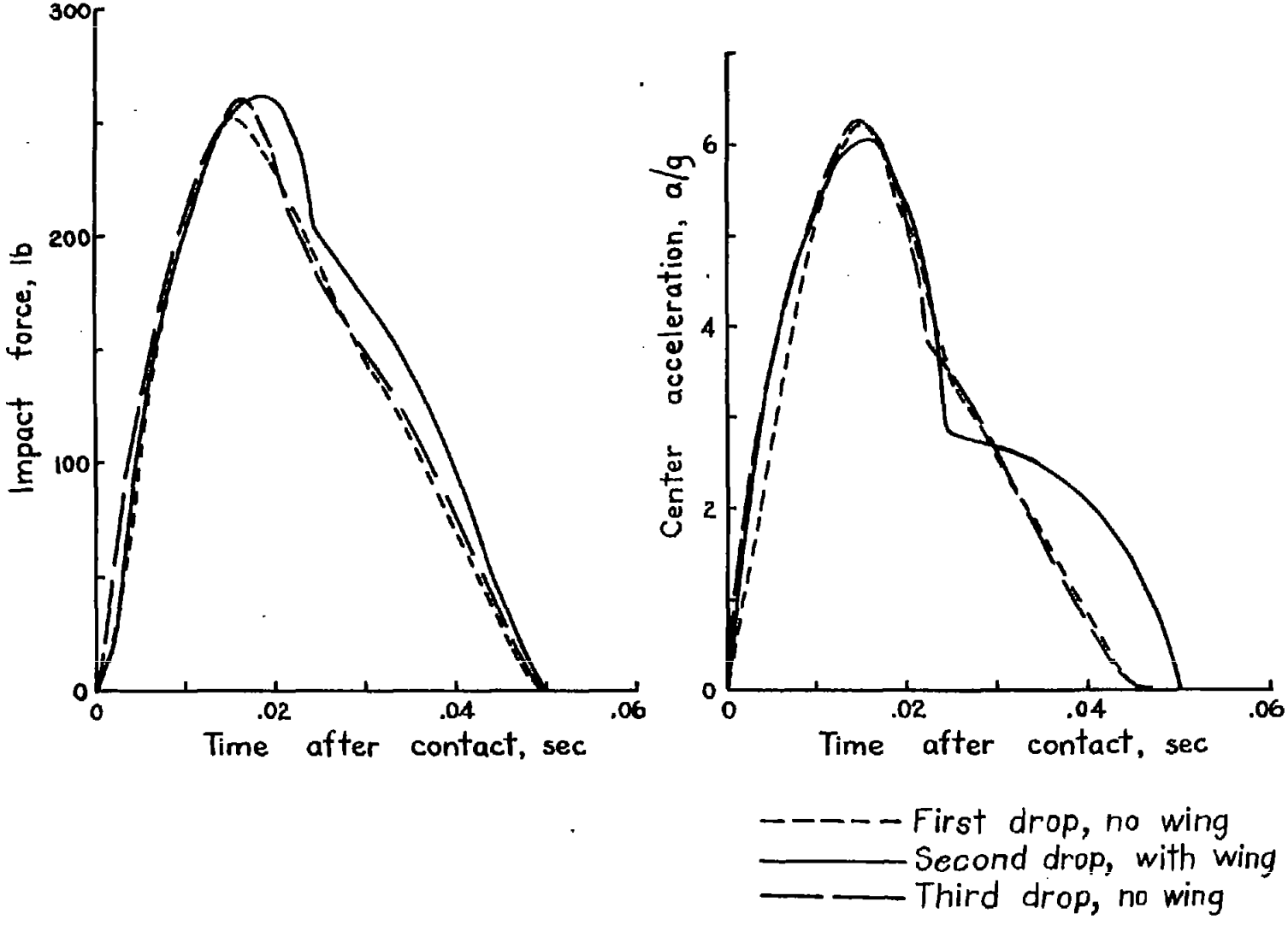

Figure 12.- Impact force and center acceleration in drops of series 7. Condition Ac, 3.52 pounds at wing tip, hard landing.

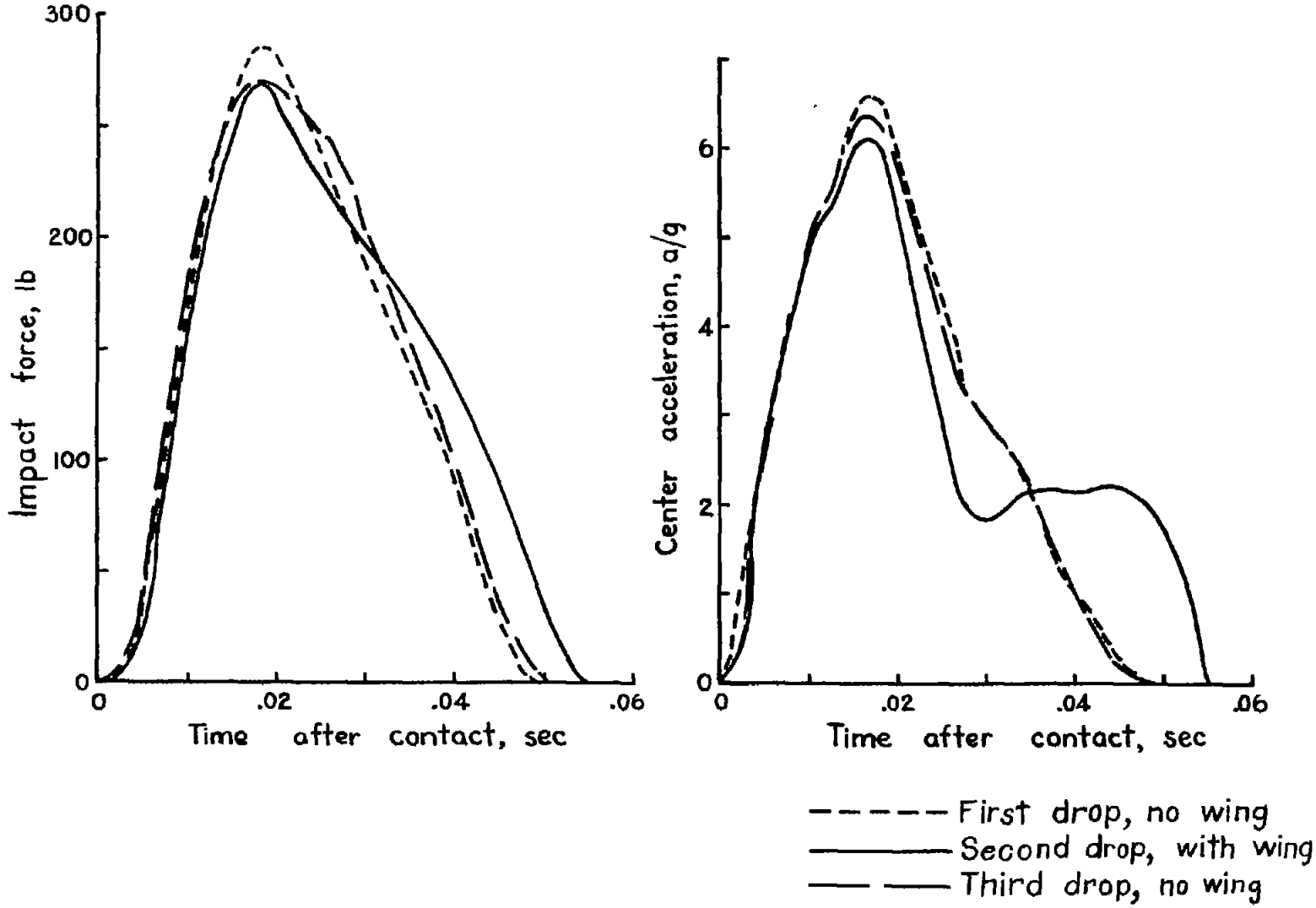

Figure 13.- Impact force and center acceleration in drops of series 8. Condition Bc, 4.52 pounds at wing tip, hard landing.

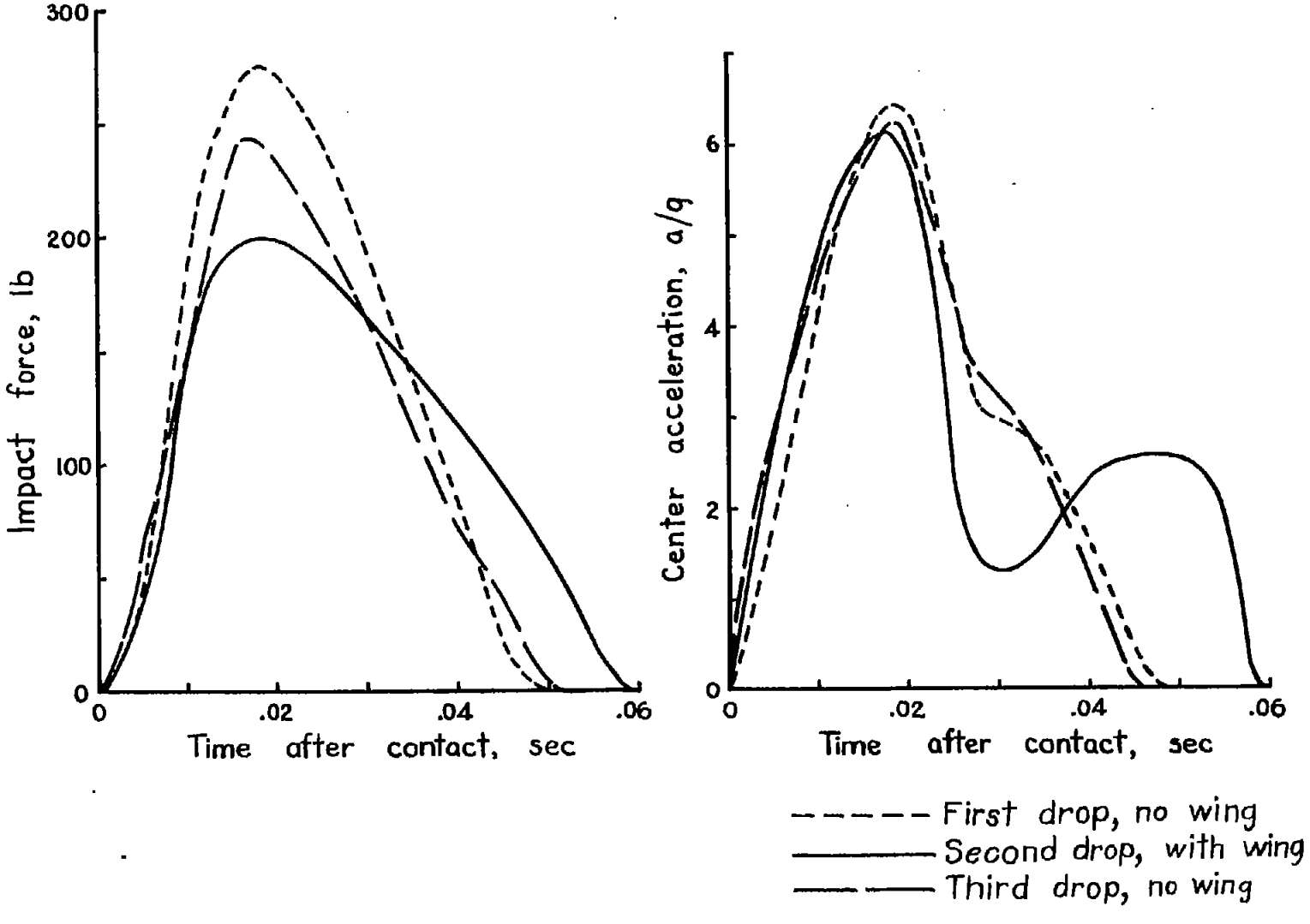

Figure 14.- Impact force and center acceleration in drops of series 9. Condition Cc, 5.52 pounds at wing tip, hard landing.

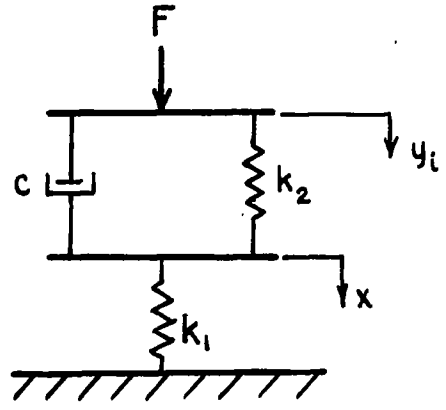

Figure 15.- Idealized landing gear. Tire represented by linear spring k_1, air chamber by linear spring k_2, oil by viscous damper c, tire deflection by x, and landing-gear deflection by y_i.

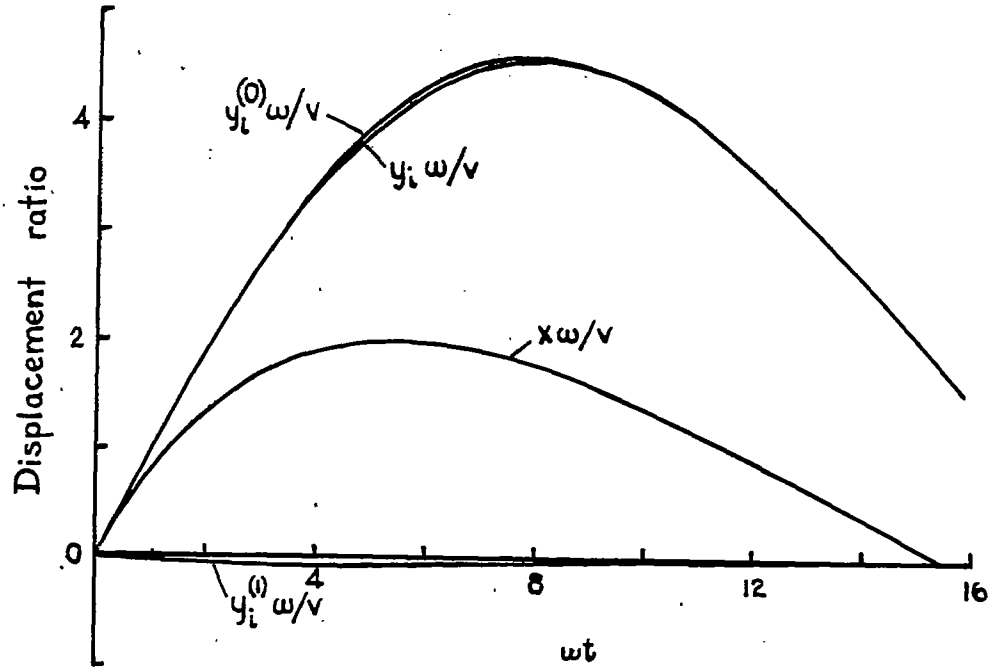

Figure 16.- Computed displacements for case 2, table 3.

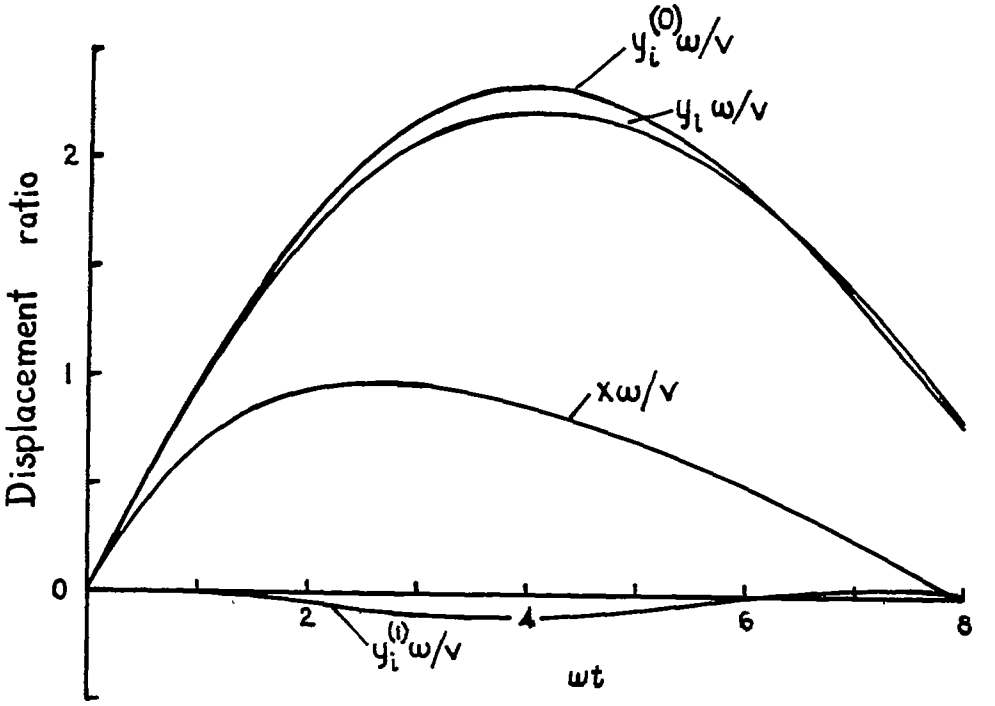

Figure 17.- Computed displacements for case 4, table 3.

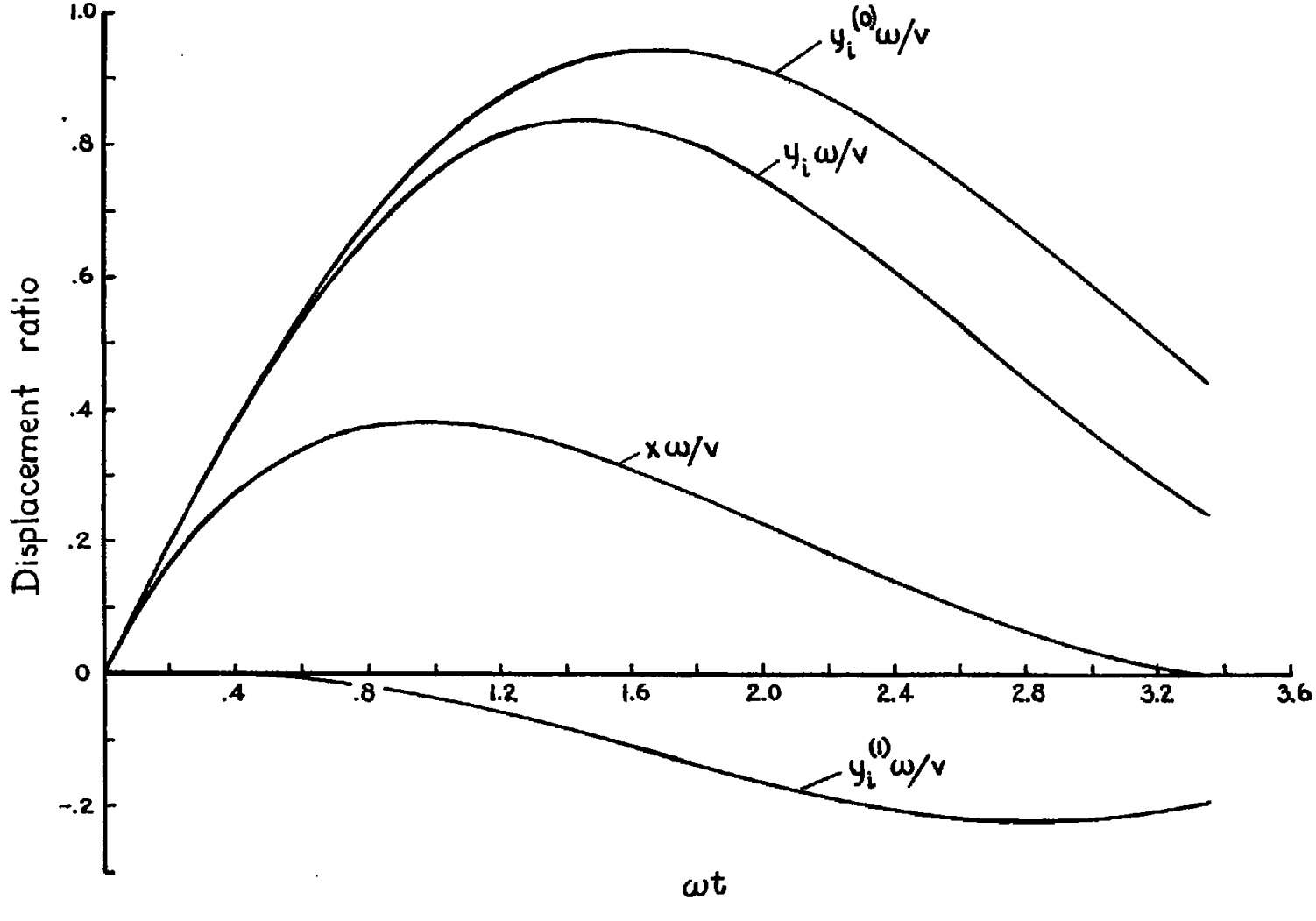

Figure 18.- Computed displacements for case 6, table 3.

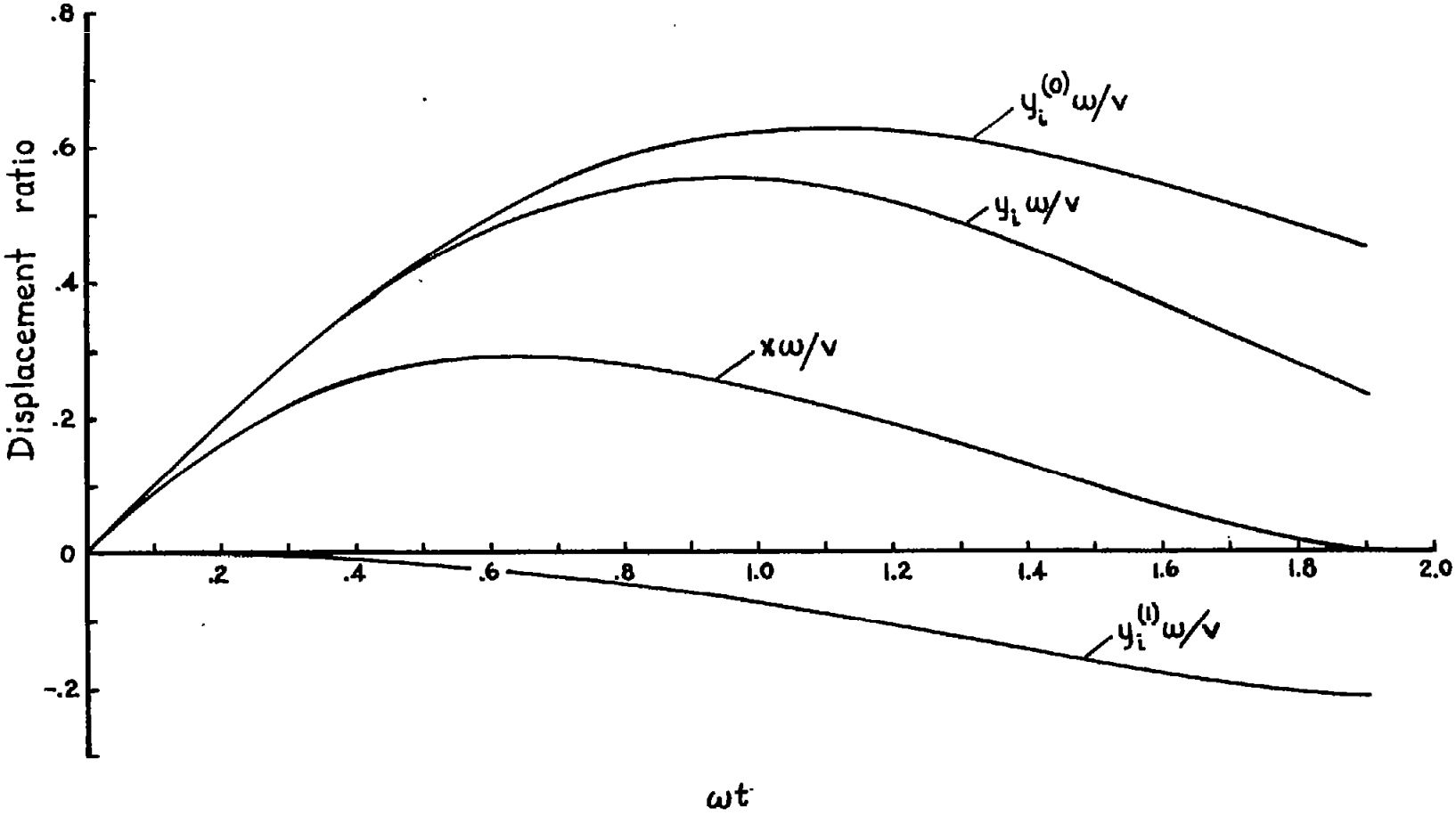

Figure 19.- Computed displacements for case 14, table 3.

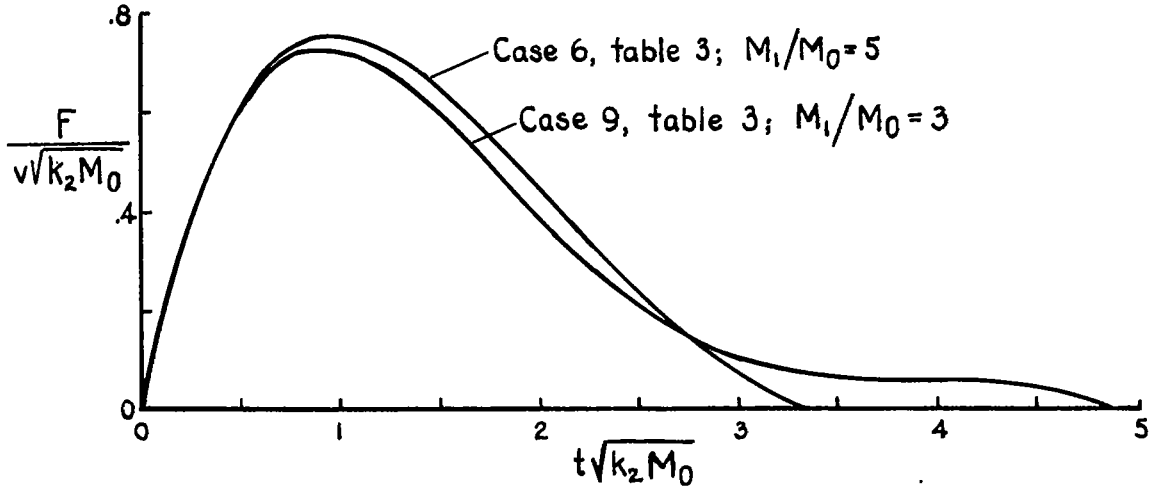

Figure 20.- Effect of mass distribution on impact-force ratio $\frac{F}{v\sqrt{k_2 M_0}}$ for durations of impact less than natural period of wing.

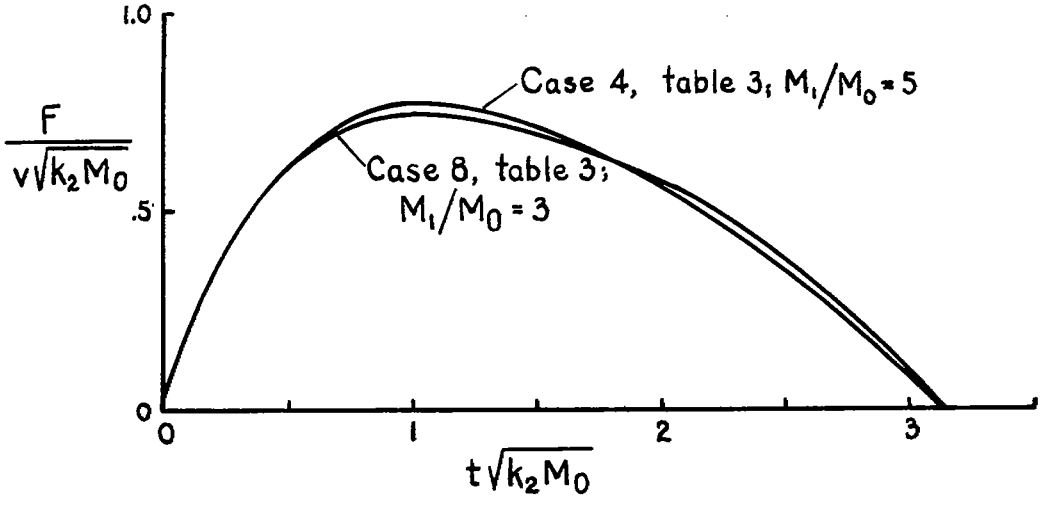

Figure 21.- Effect of mass distribution on impact-force ratio $\frac{F}{v\sqrt{k_2 M_0}}$ for durations of impact greater than natural period of wing.

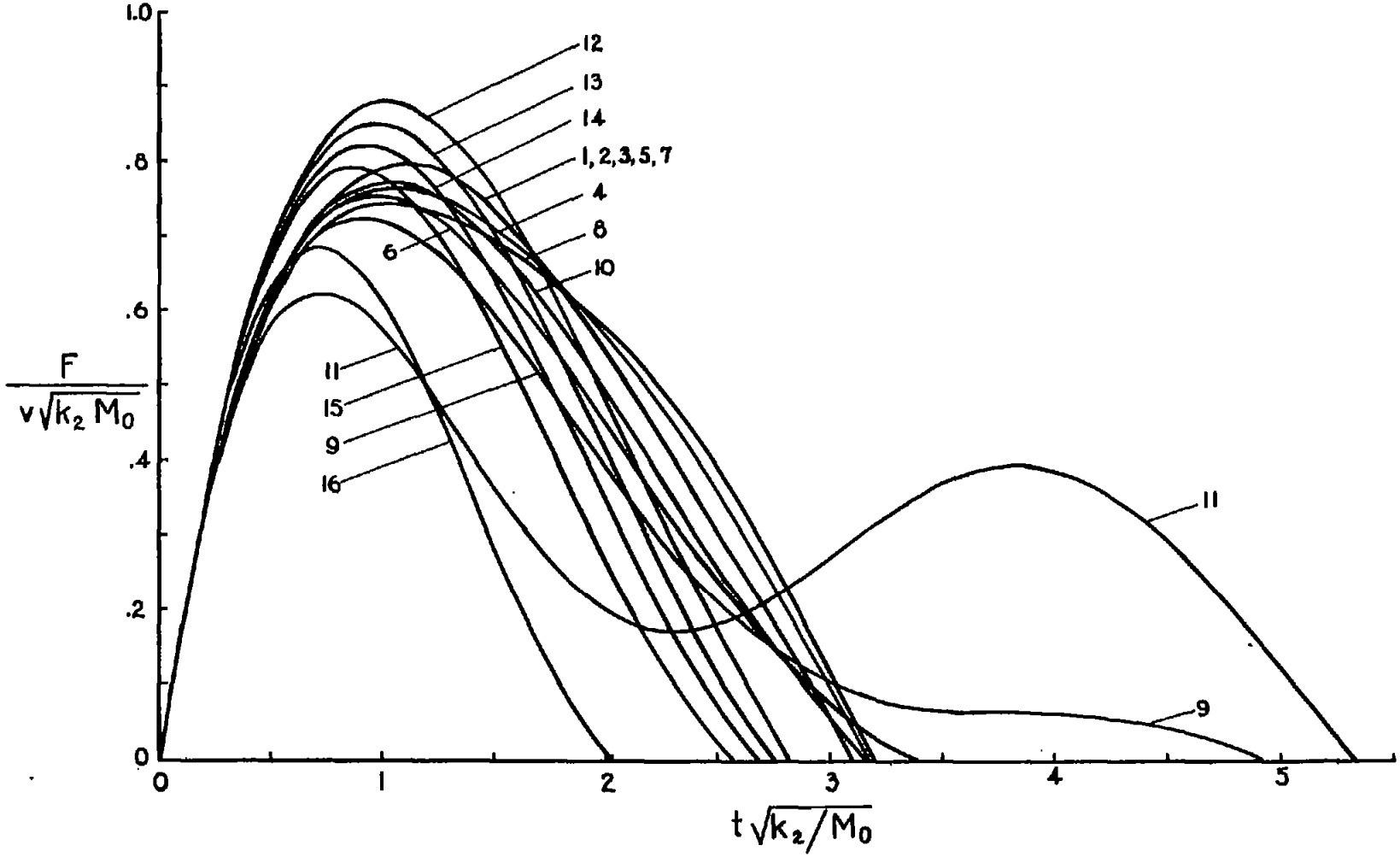

Figure 22.- Dimensionless impact force against time. Numbers designating curves correspond to cases tabulated in table 3.